DOI: 10.61782/fa.2025.0721

FORUM ACUSTICUM
EURONOISE 2025

QUANTIFYING THE IMPACT OF INJECTION MOLDING PROCESS PARAMETERS ON THE VIBROACOUSTIC PERFORMANCE OF MANUFACTURED LOCALLY RESONANT METAMATERIALS

Alara Karaman[1,2*] **Lucas Van Belle**[2,3] **Elke Deckers**[1,2]

[1] Department of Mechanical Engineering, Campus Diepenbeek, KU Leuven, Belgium
[2] Flanders Make@KU Leuven, Belgium
[3] Department of Mechanical Engineering, KU Leuven, Belgium

ABSTRACT

Locally resonant metamaterials (LRMs) have recently emerged as a promising solution which can combine lightweight design with effective noise and vibration control. These LRMs, typically consisting of a host structure with sub-wavelength added resonators, are often manufactured using additive manufacturing, which is unsuitable for mass production. Moreover, the manufacturing process can significantly affect the performance of LRMs, leading to differences between their intended design and actual results. Injection molding (IM) has been recently explored as an alternative that is suitable for mass manufacturing of LRMs though it still may affect performance.

This study focuses on how IM process parameters such as injection and packing pressure, mold and melt temperature, cooling and packing time, and injection speed influence the vibration attenuation in LRMs by investigating their impact on the effective modal parameters of the resonator and on the predicted stop band. A framework is proposed which iteratively calculates these objectives and uses single and multi-objective Bayesian approaches to determine its upper and lower bounds with respect to variation in the process parameters. These process parameters are found to have a significant impact on the vibroacoustic behavior of the LRMs, which may also be leveraged further in view of broadband vibration attenuation.

*__Corresponding author__: alara.karaman@kuleuven.be.

Keywords: *metamaterials, injection molding, uncertainty*

1. INTRODUCTION

Industry has a clear trend toward lightweight designs mainly due to economic and ecological reasons; however, traditional noise and vibration mitigation strategies typically rely on adding mass or volume, which leads to heavy and bulky solutions. This not only increases emissions during transport but also contradicts the trend towards lightweight design. In contrast, LRMs offer a lightweight and targeted approach to addressing noise and vibration issues.

In literature, LRMs have been manufactured using additive manufacturing [1–3], which has advantages like rapid prototyping but is not suitable for mass production. For metals, manufacturing techniques such as punching and bending [4], milling [5], and waterjet cutting [6] are utilized. Additionally, laser cutting [7] and thermoforming [8] are other alternatives. Some recent studies [9, 10] also investigated injection molding (IM) for LRM production, which is one of the most common techniques for mass manufacturing plastics. Manufacturing variability is inherent due to real-world engineering conditions [11], which may affect robustness.

In a previous study, it was shown that incorporating IM simulations during the design of an injection-molded metamaterial can improve the predicted performance [10]. It is also well known that the machine process variables in the IM process significantly impact product quality, particularly in terms of warpage and shrinkage deformations

[12], as well as part weight [13]. In particular, process parameters influence warpage, shrinkage, and material variability. In this study, we propose an approach to evaluate the potential influence of operational parameter ranges by combining a numerical prediction workflow [10] for the as-produced metamaterial performance with an interval uncertainty quantification approach.

In what follows, first in Sec. 2 a brief description of the metamaterial design is given. Sec. 3 outlines the approaches used to calculate the performance metrics and bounds. Sec. 4 introduces the model and presents the results. Finally, Sec. 5 discusses the main findings and gives the future perspectives.

2. THE METAMATERIAL DESIGN

An LRM plate is investigated, which consists of a 50 mm square aluminum (aluminum 6061) plate with a 1.5 mm thickness as the unit cell host structure and periodically added dual-cantilever polypropylene (PP) resonators. The resonator C [10] is chosen for analysis using the same geometric parameters employed in the study, with a first combined bending eigenfrequency tuned nominally around 1154 Hz.

3. METHODOLOGY

In this section, the numerical performance prediction flow is explained, the performance metrics to be used in this study are introduced, and approaches to find the performance bounds are briefly discussed.

3.1 Injection Molding Simulations

The machine process parameters to be varied are injection and packing pressure, mold and melt temperature, cooling and packing time, and injection speed. For the specific parameters, filling, packing, and warpage processes are simulated with MOLDEX3D 2023 using a boundary layer mesh (BLM) of the part. Then, this BLM mesh is exported, including the material cards that may differ in density across the elements in the mesh.

Two approaches have been studied for performance predictions: Approach 1 for modal parameter estimation and Approach 2 for stop-band predictions. These two approaches are summarized in Fig. 1.

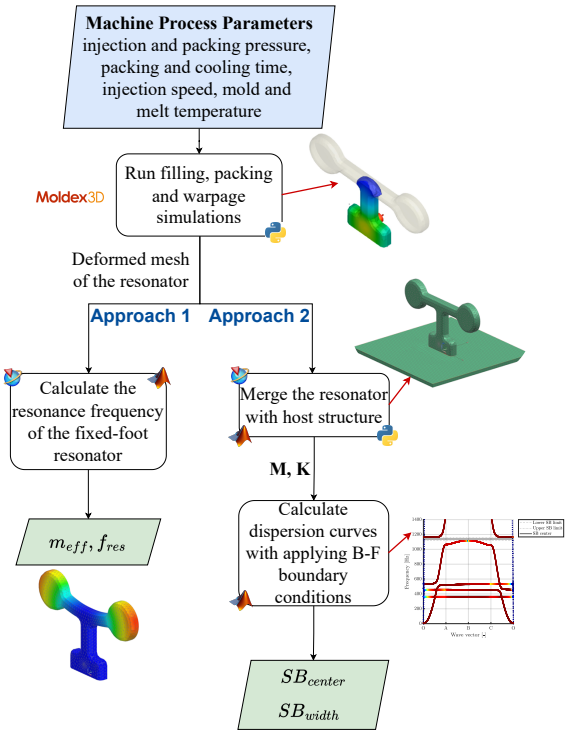

Figure 1: The flowchart of the performance prediction calculations for modal parameters (Approach 1) and stop-band predictions (Approach 2).

3.2 Approach 1: Modal Parameter Estimation

Two key modal parameters for LRM design are chosen as performance metrics: the resonator's eigenfrequency (f_{res}) and its modal effective mass (m_{eff}). The eigenfrequency of the resonator directly affects the stop-band center. On the other hand, as the m_{eff} of the resonator increases, larger stop-band widths can be achieved [14]. Hence, it is crucial to know how these metrics vary if the performance of LRMs is to be assessed.

These metrics will be computed for the resonator with clamped boundary conditions on its foot elements. The nodes corresponding to the resonator foot bottom are automatically selected and fixed for the deformed resonator mesh with variable density information exported from the injection molding simulations. Then, the f_{res} and m_{eff} are calculated by solving the corresponding eigenvalue problem. The automatization of this resonator performance prediction, Approach 1, was implemented using NX open scripts created in Python.

3.3 Approach 2: Stop-band Predictions

Ultimately, to evaluate the performance of the LRMs, m_{eff} and f_{res} may not provide the full story. Therefore, Approach 2 is employed for the stop-band predictions.

First, the deformed resonator is merged with the host structure using conformal meshes by projecting foot elements of the resonator to the unit cell of the plate host structure. Automation for this task is again done using an NX-open script created in Python. Then, applying Bloch-Floquet boundary conditions to the boundaries of the unit cell, the dispersion curves of the infinite periodic structure are calculated along the irreducible Brillouin contour (IBC). A reduced unit cell model technique known as Generalized Bloch Mode Synthesis (GBMS) [15] is used to save computational time. Finally, stop-band characteristics (SB_{center} and SB_{width}) are extracted using the resulting dispersion curves. For a more in-depth explanation of the stop-band calculation procedure, the reader is referred to [16].

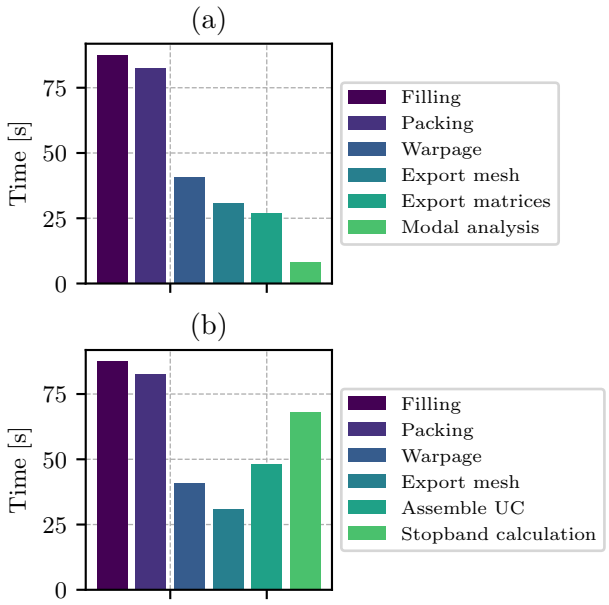

Figure 2: Overview of the time taken for (a) Approach 1, (b) Approach 2.

The steps in Sec. 3.1 and Sec. 3.2 for Approach 1, and Sec. 3.1 and Sec. 3.3 for Approach 2, are sequentially connected to formulate the objective (black-box) function that is to be iterated throughout the optimization step.

3.4 Calculating the Performance Bounds

Recently, Van Belle et al. [17] used interval descriptions of the uncertain resonator parameters to investigate the interval description of the performance metrics. A similar approach is applied here, but this time, instead of the resonator design parameters, the defined seven machine process parameters of IM are used as the bounded input parameters, which would lead to bounds to be found on the performance metrics. This has the advantage of not requiring knowledge of input distributions, allowing one to rely on ranges, tolerances, common sense, or physical constraints; however, the disadvantage is that this method results in only bounds on the performance metrics as output. Nevertheless, this method offers a useful first approximation of how significantly the process parameters influence the performance of LRMs. The objective function for this problem is defined as the calculation of the minimum and maximum values of the performance parameters (minimum and maximum of Approaches 1 and 2) according to the uncertain input interval.

The computation costs for one full evaluation using Approach 1 and Approach 2 are shown in Fig. 2. Due to these computational costs, performing a large number of evaluations for the 7-dimensional parameter space would rapidly become time-consuming. A sampling-based approach, such as quasi-random sampling, typically requires many samples, leading to numerous full simulations. Additionally, it may fail to effectively identify the performance bounds, as it may not cover the entire input space. On the other hand, given the small number of parameters, a similar surrogate modeling technique from the aforementioned study, based on Gaussian processes (GP) and Bayesian optimization (BO), can be leveraged, as it offers an efficient framework for propagating interval-uncertain parameters when there is limited number of uncertain parameters while effectively decreasing the number of simulations to be run.

The methodology of this combined BO and GP approach can be summarized as follows [18]: For a training set, based on a limited number of full simulations, a GP model of the objective function is created. This GP model acts as a hypersurface that approximates the objective function across the entire parameter space. Using this GP model, an acquisition function (AF) can be efficiently minimized to find the likely optimum, which is the potential minimum of the objective function. Depending on the AF used, the likely optimum might be based on local GP mean, uncertainty, or confidence bounds. After the most

promising parameter combination is identified with this AF, a new full simulation is run at that parameter combination. This new data point is then added to the training set, and the GP model is updated accordingly. The process then reiterates, with the updated GP model potentially suggesting even better optimals, until a stopping criterion is met, which is the maximum number of evaluations in this case.

3.4.1 Single Objective Bayesian Approach

For Approach 1, the bounds on the resulting performance metrics at the resonator level, f_{res} and m_{eff} can be computed by the following four optimization problems:

$$\begin{aligned} m_{eff,LB} &= \min\{m_{eff}(\mathbf{p}) \mid \mathbf{p}_{\min} \leq \mathbf{p} \leq \mathbf{p}_{\max}\} \\ m_{eff,UB} &= \max\{m_{eff}(\mathbf{p}) \mid \mathbf{p}_{\min} \leq \mathbf{p} \leq \mathbf{p}_{\max}\} \\ f_{res,LB} &= \min\{f_{res}(\mathbf{p}) \mid \mathbf{p}_{\min} \leq \mathbf{p} \leq \mathbf{p}_{\max}\} \\ f_{res,UB} &= \max\{f_{res}(\mathbf{p}) \mid \mathbf{p}_{\min} \leq \mathbf{p} \leq \mathbf{p}_{\max}\} \end{aligned} \tag{1}$$

where $\mathbf{p}_{\min} \leq \mathbf{p} \leq \mathbf{p}_{\max}$ denotes a vector inequality, i.e., $(p_{\min})_i \leq p_i \leq (p_{\max})_i$ for every $i = 1, 2, \ldots, 7$ defined for the input space for process parameters.

Single-objective BO with GP is applied separately to each objective function to determine the bounds for each modal performance parameter. The acquisition function is selected as the lower confidence bound. This is implemented using the *bayesopt* function in MATLAB, and a *bounding box* is created for the model performance metrics, which demarks the bounded region in the m_{eff}-f_{res} space. An initial training set of 27 full simulations is run, with the corresponding 27 parameter combinations generated through the Halton sequence using the MATLAB function *haltonset*. The stopping criterion is set at a total of 108 model evaluations for each corner of the *bounding box*.

3.4.2 Multi Objective Bayesian Approach

Instead of calculating the *bounding box*, the *bounding envelope* can be calculated if multiobjective optimization is used to calculate the Pareto optimal. Assuming a convex bounding envelope, the f_{res} and m_{eff} space is divided into four quadrants, and the Pareto front for each of these quadrants is sought by the following optimization problems:

$$\begin{aligned} f_{Q1} &= \min\{\begin{matrix}-m_{eff}(\mathbf{p}) \\ f_{res}(\mathbf{p})\end{matrix} \mid \mathbf{p}_{\min} \leq \mathbf{p} \leq \mathbf{p}_{\max}\} \\ f_{Q2} &= \min\{\begin{matrix}-m_{eff}(\mathbf{p}) \\ -f_{res}(\mathbf{p})\end{matrix} \mid \mathbf{p}_{\min} \leq \mathbf{p} \leq \mathbf{p}_{\max}\} \\ f_{Q3} &= \min\{\begin{matrix}m_{eff}(\mathbf{p}) \\ -f_{res}(\mathbf{p})\end{matrix} \mid \mathbf{p}_{\min} \leq \mathbf{p} \leq \mathbf{p}_{\max}\} \\ f_{Q4} &= \min\{\begin{matrix}m_{eff}(\mathbf{p}) \\ f_{res}(\mathbf{p})\end{matrix} \mid \mathbf{p}_{\min} \leq \mathbf{p} \leq \mathbf{p}_{\max}\} \end{aligned} \tag{2}$$

For this, a multiobjective Bayesian algorithm called TSEMO [19] is used. The stopping criteria is set to a total of 120 model evaluations per quarter, with a different set of 27 initial random data points generated through Latin hypercube sampling (LHS) for each quarter.

4. CASE STUDY

A BLM with 5 boundary layers with 1 mm node seed is used, resulting in 33949 elements. After the injection molding simulations, the mesh with variable material cards is exported using the dedicated finite element export option in MOLDEX3D. Similar to [10], density is reduced so that a minimum of 30 different material cards are exported to reduce computational time. The mesh of the resonator is given in Fig. 3.

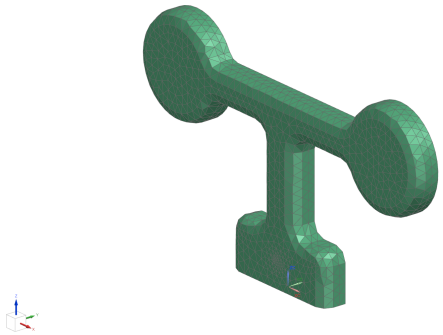

Figure 3: The resonator mesh

The machine process parameter ranges to be examined are listed in Tab. 1.

4.1 Resonator Performance Bounds

A prestudy is conducted using a random Halton dataset and an orthogonal Taguchi array with 14 levels. The total number of model evaluations is set to 196 for the Halton

Table 1: Machine process parameter ranges

Parameter	Low Bound	High Bound
Injection pressure [MPa]	100	180
Packing pressure [MPa]	100	170
Packing time [s]	1	20
Cooling time [s]	1	20
Injection speed [cm^3/s]	10	40
Mold temperature [°C]	40	70
Melt temperature [°C]	220	270

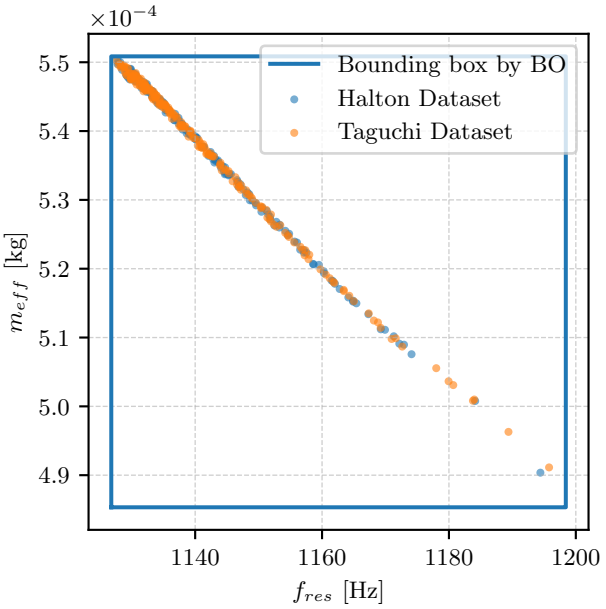

Figure 4: The bounding box calculated by single objective Bayesian optimization, together with 197 different data points calculated by Taguchi array and Halton Sequence.

dataset, based on the corresponding Taguchi array with 7 levels.

Fig. 4 gives the overview of single objective optimization and sampling results. The relationship between the resonator's eigenfrequency and modal effective mass appears to be quite linear, based on sampling. Finding the separate individual bounds shows that the samples are all within these bounds. However, the bounding box, which is now necessarily a rectangle, loses that clear trend. Thus, although interesting and promising, the multiobjective approach could give more insights.

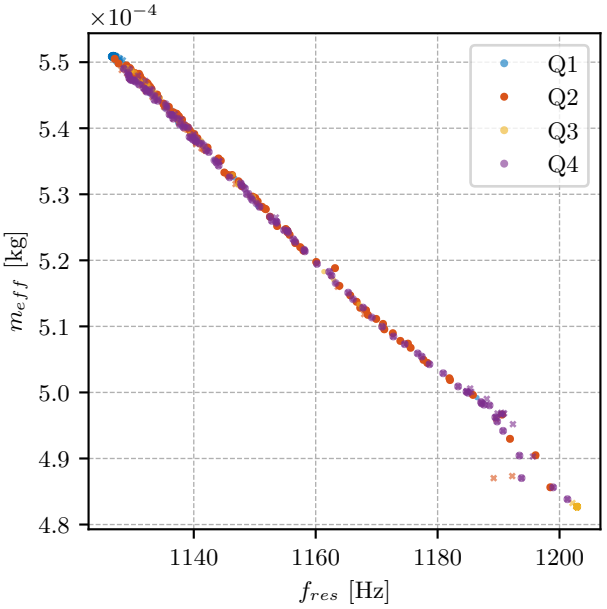

Figure 5: The bounding envelope calculated by multi-objective Bayesian optimization.

Fig. 5 gives an overview of the multi-objective optimization results. In comparison with Fig. 4, it shows that only a few samples are in the bottom-right corner, while most are clustered in the middle to top-left regions. This suggests that the parameter range leading to the bottom-right region is potentially narrow or scattered, making it harder to capture. While the BO algorithm performs well in the middle and top-left, refining the acquisition function, kernel, or objective function may help improve results in the bottom-right.

4.2 Stop-band Performance Bounds

A Taguchi sampling-based approach is done on the stop-band performance to present an initial impression in this paper. Fig. 6 shows an overview of the stop-band predictions. As is well-known from metamaterial design, the SB_{center} is highly correlated with f_{res}, which is also seen on Fig. 6, while the SB_{width} depends on the (effective) mass of the resonator. Moreover, a broader stop-band with increasing frequency is typically expected. However, in this case, the increasing frequency corresponds to, and may even be caused by, a reduced resonator ef-

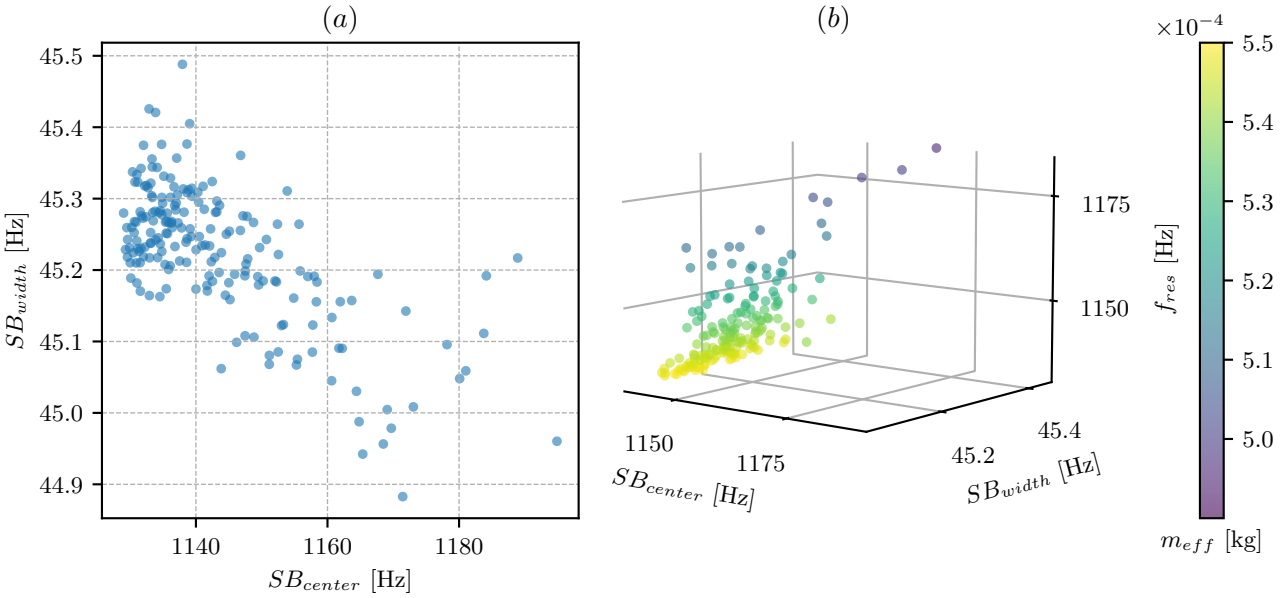

Figure 6: (a) Approach 2 metrics calculated with the Taguchi sample (b) combined resonator (Approach 1) and stop band (Approach 2) metrics plotted together.

fective mass. In Fig. 6, the stop-band width slightly decreases (yet remains almost constant), suggesting that, at the LRM level, both of these effects may, to some extent, counterbalance each other for this example.

5. CONCLUSIONS

In this paper, two approaches for assessing the IM variability are proposed for LRMs. These approaches iteratively calculate the LRM performance, either at the resonator level or at the unit cell level, to investigate the influence of manufacturing variability effects of IM.

The machine operation parameters of the IM process are shown to have a clear effect on the vibroacoustic performance of the LRMs and the targeted frequency range of the resonator. For the given case study, with the variation in process parameters shown in Tab. 1, an approximately 3% variation in frequency and 6% variation in effective mass of the resonator can be observed from Fig. 5. This variation could be utilized further for broadband attenuation.

Although the bounding box indicates bounds on individual performance metrics well, trends that may exist between dependent performance metrics are lost. Using a Pareto multi-objective BO optimization showed great potential in more accurately capturing the performance bounds in LRMs.

Further investigation is required for more definitive conclusions, as the results for Approach 1 need more analysis, and the results for Approach 2 are still very preliminary and indicative. However, this framework shows promising potential for investigating manufacturing variability. In future work,

- a qualitative study will be conducted on each parameter to assess the contribution and importance of individual machine parameters versus their combined impact.
- the analysis of resonator metrics will be further expanded, including stiffness, to explain frequency variation better.
- the scope will be extended to include material property variation besides purely manufacturing process settings.

6. ACKNOWLEDGMENTS

The European Commission is gratefully acknowledged for their support of the METAVISION research project (GA 101072415). Views and opinions expressed are,

however, those of the authors only and do not necessarily reflect those of the European Union. The European Union cannot be held responsible for them. The research of L. Van Belle (fellowship no. 1254325) is funded by a grant from the Research Foundation – Flanders (FWO). Internal Funds KU Leuven are gratefully acknowledged for their support.

7. REFERENCES

[1] C. Claeys, E. Deckers, B. Pluymers, and W. Desmet, "A lightweight vibro-acoustic metamaterial demonstrator: Numerical and experimental investigation," *Mechanical Systems and Signal Processing*, vol. 70–71, pp. 853–880, 2016.

[2] L. Sangiuliano, C. Claeys, E. Deckers, J. De Smet, B. Pluymers, and W. Desmet, "Reducing Vehicle Interior NVH by Means of Locally Resonant Metamaterial Patches on Rear Shock Towers," in *SAE Technical Paper*, pp. 2019–01–1502, 2019.

[3] S. Tomita, T. Masutani, and H. Sato, "Locally resonant metamaterials damped by particles embedded through additive manufacturing," *Journal of Sound and Vibration*, vol. 596, p. 118715, 2025.

[4] M. Droste, D. Manushyna, S. Rieß, H. Atzrodt, T. Druwe, S. Melzer, A. Struß, and A. Lühring, "Design and validation of production-suited vibroacoustic metamaterials for application in a vehicle door," in *Fortschritte der Akustik - DAGA 2021*, p. 1647, 2021.

[5] L. Sangiuliano, R. Boukadia, E. Deckers, W. Desmet, and C. Claeys, "Reduction of Structure-Borne Tyre/Road Noise through Rubber Resonant Metamaterials in Tyres," *SAE International Journal of Advances and Current Practices in Mobility*, vol. 5, no. 2, pp. 909–920, 2022.

[6] S. Rieß, R. Schmidt, W. Kaal, H. Atzrodt, and S. Herold, "Vibration Reduction on Circular Disks with Vibroacoustic Metamaterials," *Applied Sciences*, vol. 14, no. 11, p. 4637, 2024.

[7] L. Van Belle, C. Claeys, E. Deckers, and W. Desmet, "On the impact of damping on the dispersion curves of a locally resonant metamaterial: Modelling and experimental validation," *Journal of Sound and Vibration*, vol. 409, pp. 1–23, 2017.

[8] N. De Melo Filho, C. Claeys, E. Deckers, and W. Desmet, "Realisation of a thermoformed vibro-acoustic metamaterial for increased STL in acoustic resonance driven environments," *Applied Acoustics*, vol. 156, pp. 78–82, 2019.

[9] J. Yu, C. Nerse, G. Lee, S. Wang, and K.-j. Chang, "Mass Production Applicable Locally Resonant Metamaterials for NVH Applications," in *26th International Congress on Sound and Vibration*, 2019.

[10] K. Steijvers, C. Claeys, L. Van Belle, and E. Deckers, "Incorporating Manufacturing Process Simulations to Enhance Performance Predictions of Injection Moulded Metamaterials," *Journal of Vibration Engineering & Technologies*, vol. 11, no. 6, pp. 2617–2629, 2023.

[11] S. Cantero-Chinchilla, A. T. Fabro, H. Meng, W.-J. Yan, C. Papadimitriou, and D. Chronopoulos, "Robust optimised design of 3D printed elastic metastructures: A trade-off between complexity and vibration attenuation," *Journal of Sound and Vibration*, vol. 529, p. 116896, 2022.

[12] N.-y. Zhao, J.-y. Lian, P.-f. Wang, and Z.-b. Xu, "Recent progress in minimizing the warpage and shrinkage deformations by the optimization of process parameters in plastic injection molding: A review," *The International Journal of Advanced Manufacturing Technology*, vol. 120, no. 1-2, pp. 85–101, 2022.

[13] H. Hassan, "An experimental work on the effect of injection molding parameters on the cavity pressure and product weight," *The International Journal of Advanced Manufacturing Technology*, vol. 67, pp. 675–686, July 2013.

[14] F. Pires, R. Boukadia, M. Wandel, C. Thomas, E. Deckers, W. Desmet, and C. Claeys, "Novel resonator concept for improved performance of locally resonant based metamaterials," *Thin-Walled Structures*, vol. 209, p. 112866, 2025.

[15] D. Krattiger and M. I. Hussein, "Generalized Bloch mode synthesis for accelerated calculation of elastic band structures," *Journal of Computational Physics*, vol. 357, pp. 183–205, Mar. 2018.

[16] L. Van Belle, N. Filho, M. Clasing, C. Claeys, E. Deckers, F. Naets, and W. Desmet, "Fast metamaterial design optimization using reduced order unit cell modeling," in *Proceedings of ISMA 2020*, p. 2487–2501, 2020.

[17] L. Van Belle, E. Deckers, and A. Cicirello, "Investigating and exploiting the impact of variability in resonator parameters on the vibration attenuation in locally resonant metamaterials," *Philosophical Transactions of the Royal Society A: Mathematical, Physical and Engineering Sciences*, vol. 382, no. 2279, p. 20230364, 2024.

[18] A. Cicirello and F. Giunta, "Machine learning based optimization for interval uncertainty propagation," *Mechanical Systems and Signal Processing*, vol. 170, p. 108619, 2022.

[19] E. Bradford, A. M. Schweidtmann, and A. Lapkin, "Efficient multiobjective optimization employing Gaussian processes, spectral sampling and a genetic algorithm," *Journal of Global Optimization*, vol. 71, no. 2, pp. 407–438, 2018.